



**HAL**  
open science

## Experimental acoustic characterisation of an endoskeletal antibubble contrast agent: first results

Anastasiia Panfilova, Peiran Chen, Ruud J.G. van Sloun, Hessel Wijkstra, Michiel Postema, Albert T. Poortinga, Massimo Mischi

► **To cite this version:**

Anastasiia Panfilova, Peiran Chen, Ruud J.G. van Sloun, Hessel Wijkstra, Michiel Postema, et al.. Experimental acoustic characterisation of an endoskeletal antibubble contrast agent: first results. Medical Physics, 2021, 10.1002/mp.15242 . hal-03338989v1

**HAL Id: hal-03338989**

**<https://hal.science/hal-03338989v1>**

Submitted on 9 Sep 2021 (v1), last revised 1 Dec 2021 (v4)

**HAL** is a multi-disciplinary open access archive for the deposit and dissemination of scientific research documents, whether they are published or not. The documents may come from teaching and research institutions in France or abroad, or from public or private research centers.

L'archive ouverte pluridisciplinaire **HAL**, est destinée au dépôt et à la diffusion de documents scientifiques de niveau recherche, publiés ou non, émanant des établissements d'enseignement et de recherche français ou étrangers, des laboratoires publics ou privés.

# Experimental acoustic characterisation of an endoskeletal antibubble contrast agent: first results

Anastasiia Panfilova<sup>1\*</sup>, Peiran Chen<sup>1</sup>, Ruud JG van Sloun<sup>1</sup>, Hessel Wijkstra<sup>1,2</sup>, Michiel Postema<sup>3,4</sup>, Albert T. Poortinga<sup>5</sup>, Massimo Mischi<sup>1</sup>

<sup>1</sup> Electrical Engineering Department, Eindhoven University of Technology, Eindhoven, The Netherlands

<sup>2</sup> Department of Urology, Amsterdam University Medical Centers location AMC, Meibergdreef 9, 1105 AZ, Amsterdam, The Netherlands

<sup>3</sup> School of Electrical and Information Engineering, University of the Witwatersrand, Johannesburg, Braamfontein, Republic of South Africa

<sup>4</sup> BioMediTech, Faculty of Medicine and Health Technology, Tampere University, Tampere, Finland

<sup>5</sup> Mechanical Engineering Department, Eindhoven University of Technology, Eindhoven, The Netherlands

Version typeset September 2, 2021

Author to whom correspondence should be addressed. email: anastasiapanfilova09@gmail.com

## Abstract

**Purpose:** An antibubble is an encapsulated gas bubble with an incompressible inclusion inside the gas phase. Current-generation ultrasound contrast agents are bubble-based: they contain encapsulated gas bubbles with no inclusions. The objective of this work is to determine the linear and nonlinear responses of an antibubble contrast agent in comparison to two bubble-based ultrasound contrast agents, *i.e.*, reference bubbles and SonoVue<sup>TM</sup>.

**Methods:** Side scatter and attenuation of the three contrast agents were measured, using single-element ultrasound transducers, operating at 1 MHz, 2.25 MHz and 3.5 MHz. The scatter measurements were performed at acoustic pressures of 200 kPa and 300 kPa for 1 MHz, 300 kPa and 450 kPa for 2.25 MHz, and 370 kPa and 560 kPa for 3.5 MHz. Attenuation measurements were conducted at pressures of 13 kPa, 55 kPa and 50 kPa for 1 MHz, 2.25 MHz, and 3.5 MHz, respectively. In addition, a dynamic contrast-enhanced ultrasound measurement was performed, imaging the contrast agent flow through a vascular phantom with a commercial diagnostic linear array probe.

**Results:** Antibubbles generated equivalent or stronger harmonic signal, compared to bubble-based ultrasound contrast agents. The 2nd harmonic side-scatter amplitude of the antibubble agent was up to 3 dB greater than that of reference bubble agent and up to 4 dB greater than that of SonoVue<sup>TM</sup> at the estimated concentration of  $8 \times 10^4$  bubbles/mL. For ultrasound with a center transmit frequency of 1 MHz, the attenuation

40 coefficient of the antibubble agent was 8.7 dB/cm, whereas the attenuation coefficient  
41 of the reference agent was 7.7 dB/cm and 0.3 dB/cm for SonoVue<sup>TM</sup>. At 2.25 MHz  
42 the attenuation coefficients were 9.7 dB/cm, 3.0 dB/cm and 0.6 dB/cm, respectively.  
43 For 3.5 MHz, they were 4.4 dB/cm, 1.8 dB/cm and 1.0 dB/cm, respectively. We hy-  
44 pothesize that the antibubble agent attenuation is greater than that of the reference  
45 agent due to the solid cores in the antibubble agent. A dynamic contrast-enhanced  
46 ultrasound recording showed the nonlinear signal of the antibubble agent to be 31%  
47 greater than for reference bubbles and 23% lower than SonoVue<sup>TM</sup> at a high concen-  
48 tration of  $2 \times 10^6$  bubbles/mL.

49 **Conclusion:** Endoskeletal antibubbles generate comparable or greater higher har-  
50 monics than reference bubbles and SonoVue<sup>TM</sup>. As a result, antibubbles with liquid  
51 therapeutic agents inside the gas phase have high potential to become a traceable ther-  
52 apeutic agent.

53

54 **Contents**

55 **I. Introduction** **1**

56 **II. Methods** **5**

57 **II.A. Scatter measurements** . . . . . 5

58 **II.A.1. Contrast agent fabrication and preparation** . . . . . 5

59 **II.A.2. Experimental procedure** . . . . . 6

60 **II.A.3. Data analysis of scatter measurements** . . . . . 8

61 **II.B. Attenuation measurements** . . . . . 9

62 **II.C. Dynamic contrast-enhanced ultrasound measurement** . . . . . 12

63 **III. Results** **14**

64 **III.A. Scattering** . . . . . 14

65 **III.B. Attenuation** . . . . . 17

66 **III.C. Dynamic contrast-enhanced ultrasound** . . . . . 18

67 **IV. Discussion** **21**

68 **V. Conclusions** **25**

69 **VI. Acknowledgements** **26**

## 1. Introduction

Ultrasound contrast agents (UCA) are utilized in the clinic in order to visualize the blood pool and assess organ perfusion and dispersion, aiding cancer detection<sup>1,2,3,4</sup>. In some cases, the current UCAs do not exhibit sufficient nonlinear behavior to eliminate clutter and image artefacts, leading to diagnostic misinterpretation<sup>5</sup>. Augmenting UCA nonlinear behavior improves image contrast and diagnostic confidence. To this end, we propose antibubbles as a new UCA. Endoskeletal antibubbles<sup>6,7</sup> have been shown to oscillate significantly more asymmetrically than reference bubbles with no cores and, therefore, are hypothesized to demonstrate enhanced nonlinear behavior compared to bubble-based UCAs.

UCAs are gas microbubbles stabilized by a shell composed of lipids, cross-linked polymers or denatured proteins<sup>8,9</sup>. With a size comparable to that of the red blood cells, they are able to pass through the smallest capillaries. At the same time, they are bigger than endothelial gaps and therefore do not extravasate into tissue<sup>10</sup>. When insonified at sufficient pressure, gas microbubbles oscillate in a nonlinear fashion, generating higher harmonics<sup>11,12</sup>. This effect is generally more pronounced when the sonicating frequency is close to the resonance frequency of the microbubbles. The generation of higher harmonics in tissue is much weaker compared to that in UCAs. This enables the implementation of contrast-specific imaging solutions for visualization of the blood pool, and therefore analysis of blood flow and vasculature by contrast-enhanced ultrasound (CE-US)<sup>13</sup> and dynamic contrast-enhanced ultrasound (DCE-US)<sup>2,4,14</sup>. Despite the recognized utility of CE-US and DCE-US in the clinic<sup>13,15</sup>, cumulative nonlinear effects occurring in tissue can reduce the contrast-to-tissue ratio, especially at greater depth<sup>5</sup>. Several contrast-specific imaging schemes, such as power modulation<sup>1,16</sup> and subharmonic imaging<sup>17,18</sup> can significantly suppress the nonlinear signal generated by tissue. In this work, we investigate the possibility of using a contrast agent with augmented nonlinear behavior for this purpose, enabling imaging at lower pressure amplitudes and causing weaker higher harmonic generation in tissue.

A droplet entrapped in a gas bubble has been referred to as an antibubble<sup>19,20</sup>. This term has also been used for UCAs with microbubbles containing incompressible inclusions in the gas phase<sup>6,21</sup>. Encapsulated microbubbles that contain incompressible inclusions and a solid supporting skeleton that suspends the inclusion have been referred to as endoskeletal antibubbles<sup>7</sup>. Figure 1 presents a schematic of an endoskeletal antibubble with a 2% volume

inclusion. Theoretical work<sup>21</sup> demonstrated antibubbles to show an increased nonlinear behavior, compared to reference gas bubbles without incompressible cores. This was attributed to non-symmetric oscillation in the US field, where the antibubble showed larger expansion than contraction because of the incompressible core. Experimental evidence of this effect was acquired with a high-speed camera for endoskeletal antibubbles<sup>7</sup>. These studies<sup>7,21</sup> suggest that antibubbles have a high potential to improve CE-US image quality, generating greater higher harmonics, compared to conventional UCAs. Besides this, antibubbles incorporating therapeutic agents in the gas phase can deliver larger doses of therapeutic agents, compared to alternative strategies<sup>8,22</sup>. This way, antibubbles may offer clinicians a traceable and highly effective therapeutic agent. Currently no clinically approved antibubble contrast agent exists. Moreover, experimental proof of greater higher-harmonic generation is scarce<sup>23</sup>. The current experimental study investigated the potential of antibubbles for imaging purposes. To this end, nonlinear side scatter and linear attenuation measurements of endoskeletal antibubbles, reference bubbles and SonoVue<sup>TM</sup> were performed in the clinically diagnostic frequency range at frequencies of 1, 2.25 and 3.5 MHz. The scatter and attenuation parameters quantify UCA efficacy: the amplitude of the nonlinear scatter signal defines the signal-to-noise ratio in DCE-US imaging, while attenuation defines the visible image depth<sup>28</sup>. The endoskeletal antibubbles have a median diameter of 6  $\mu\text{m}$ , with 93% smaller than 10  $\mu\text{m}$ <sup>24</sup> (Fig. 2a). They are stabilized by a silica shell and contain solid ZnO inclusions in the air gas phase. These inclusions take up 2% of the antibubble volume, while the rest of the gas phase contains silica nanoparticles, forming the endoskeleton<sup>7</sup> (Fig. 1). The studied endoskeletal antibubbles are somewhat bigger than those typically utilized in the clinic and, therefore, are currently only a UCA prototype. Reference bubbles have no core inclusions and no endoskeleton but, like antibubbles, have a silica shell<sup>7</sup> (Fig. 1). The median diameter of reference bubbles is 6  $\mu\text{m}$ , with 81% below 10  $\mu\text{m}$ <sup>24</sup> (Fig. 2b). The endoskeletal antibubbles and reference bubbles have not been clinically approved. Endoskeletal antibubbles are currently only an antibubble prototype, while reference bubbles give the opportunity to compare higher harmonic generation of endoskeletal antibubbles to that of a UCA with the same shell. SonoVue<sup>TM</sup> is a clinically approved UCA, used as a benchmark in this study. SonoVue<sup>TM</sup> microbubbles contain a low-solubility gas ( $\text{SF}_6$ ) encapsulated in a phospholipid shell, with a mean diameter of 3  $\mu\text{m}$ , with more than 90% of the bubbles below 8  $\mu\text{m}$ <sup>25,27</sup> (Fig. 1). Its size distribution leads to a resonance frequency around 3 MHz<sup>29,30</sup>.

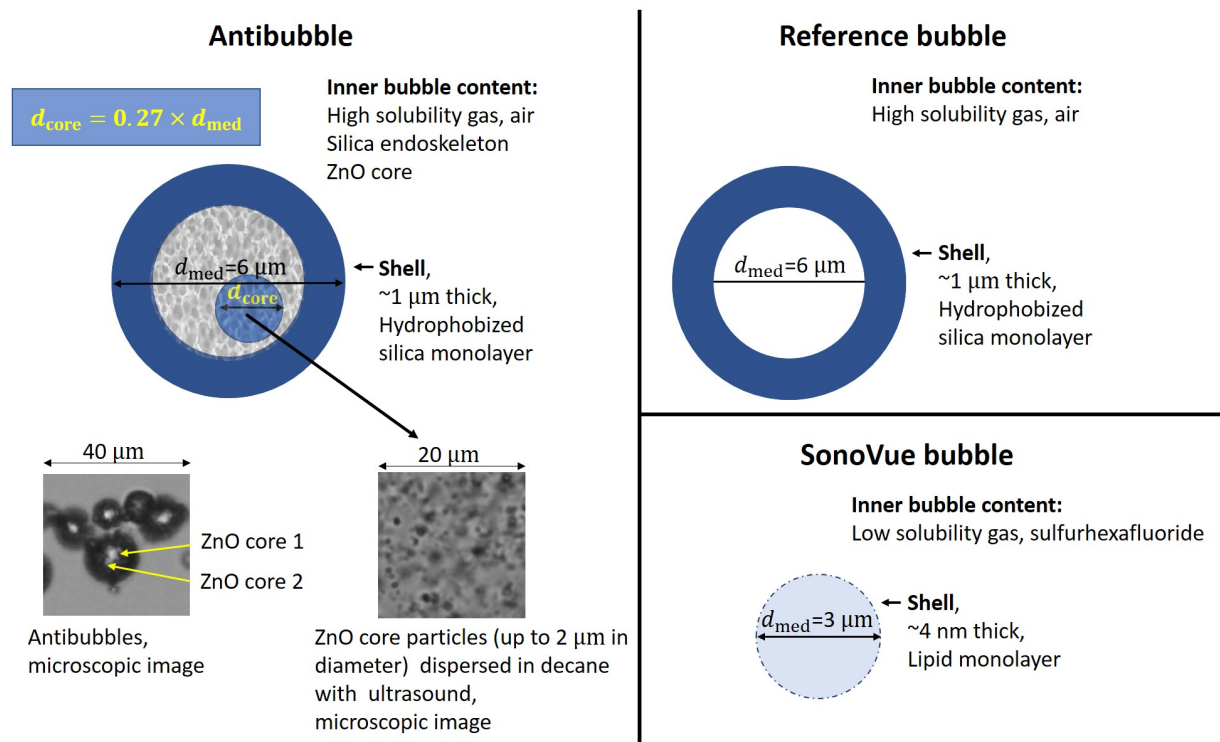


Figure 1: Schematic illustration of antibubbles, reference and SonoVue bubbles. The median antibubble diameter was estimated to be 6  $\mu\text{m}$ <sup>24</sup>. The incompressible core(s) comprises, on average, 2% volume, equivalent to an inclusion radius constituting 27 % of the bubble radius. Surrounding the core is the endoskeleton in air, encapsulated by a silica shell, whose thickness was estimated to be around 1  $\mu\text{m}$ , estimated from microscopic images in<sup>7</sup>. The median reference bubble diameter was estimated to be 6  $\mu\text{m}$ <sup>24</sup>. Reference bubbles are filled with air, encapsulated by a silica shell. SonoVue bubble, with hexafluoride ( $\text{SF}_6$ ) gas, encapsulated by a thin phospholipid shell<sup>25,26</sup> and a mean diameter of 3  $\mu\text{m}$ <sup>25,27</sup>.

133 The resonance frequencies of endoskeletal antibubbles and reference bubbles have not yet  
134 been identified.

135 The scatter measurement was performed at acoustic pressures comparable to those em-  
136 ployed clinically at mechanical indexes (MIs) of 0.2 and 0.3, often utilized for DCE-US<sup>31,32,33</sup>.  
137 Signals at these MIs are sufficiently strong to trigger nonlinear bubble oscillation and, at the  
138 same time, low enough not to induce damage to biological tissue and bubble bursting<sup>34,35</sup>. A  
139 hydrophone was utilized as a receiver to enable registration of a broad spectrum of the scat-  
140 tered signal, including higher harmonics and subharmonics. The attenuation measurement  
141 was performed for  $\text{MI} < 0.04$ . Low pressures are typical for attenuation measurements<sup>36</sup>, they  
142 avoid depletion of the fundamental signal due to generation of higher harmonics, which is  
143 especially prominent in case of UCAs. Moreover, at greater pressures UCA bubbles may

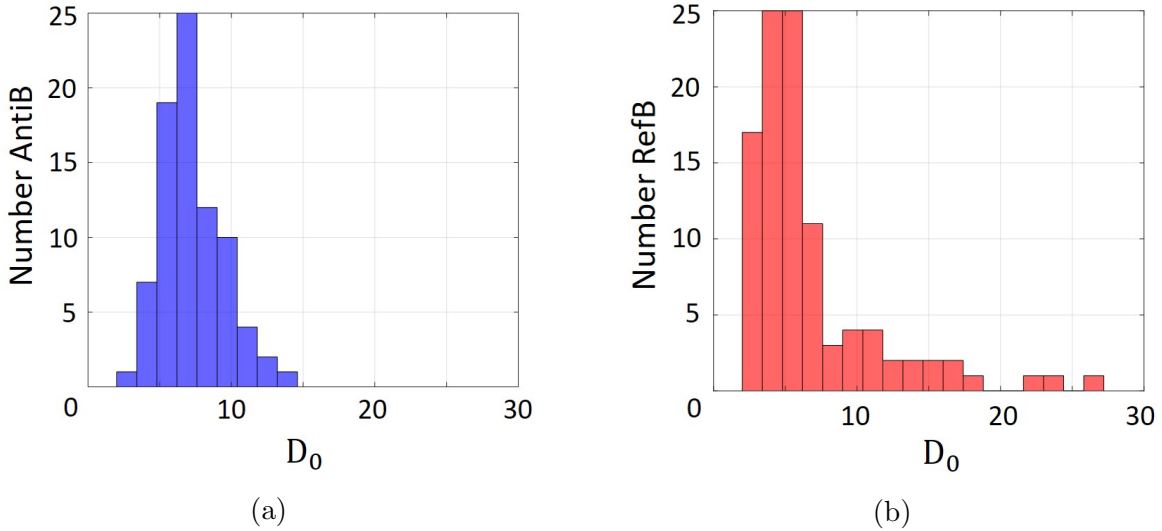


Figure 2: The size distributions of (a) antibubble and (b) reference bubble in the studied dispersions. The data was taken from (Anderton, 2020)<sup>24</sup>.

144 generate a strong fundamental component, interfering with the transmitted pulse and in-  
 145 troducing further error in the measurement. This way, we measured attenuation as a result of  
 146 energy absorption<sup>28</sup> and energy scattering in a nearly linear low-amplitude regime of bubble  
 147 oscillation<sup>37</sup>, as demonstrated for antibubbles, reference bubbles and other contrast agents  
 148 at greater pressures than those utilized in this work<sup>7,38,39</sup>. For both scatter and attenua-  
 149 tion measurement pulses of 10-20 cycles were transmitted, providing a sufficiently narrow  
 150 bandwidth to avoid overlap between the harmonics in the received spectra.

151 To demonstrate antibubbles' performance in a nearly clinical setting, a DCE-US mea-  
 152 surement was performed: the flow of endoskeletal antibubbles, reference bubbles and  
 153 SonoVue<sup>TM</sup> was imaged through a porous phantom<sup>40</sup> with a linear array US transducer.  
 154 The spaces between the acoustically transparent beads composing the vascular phantom  
 155 simulated a vascular network. The transmitted pulses consisted of 3 cycles at 3.5 MHz,  
 156 granting sufficient resolution for phantom visualization, and with an  $MI = 0.2$ .



## 157 II. Methods

### 158 II.A. Scatter measurements

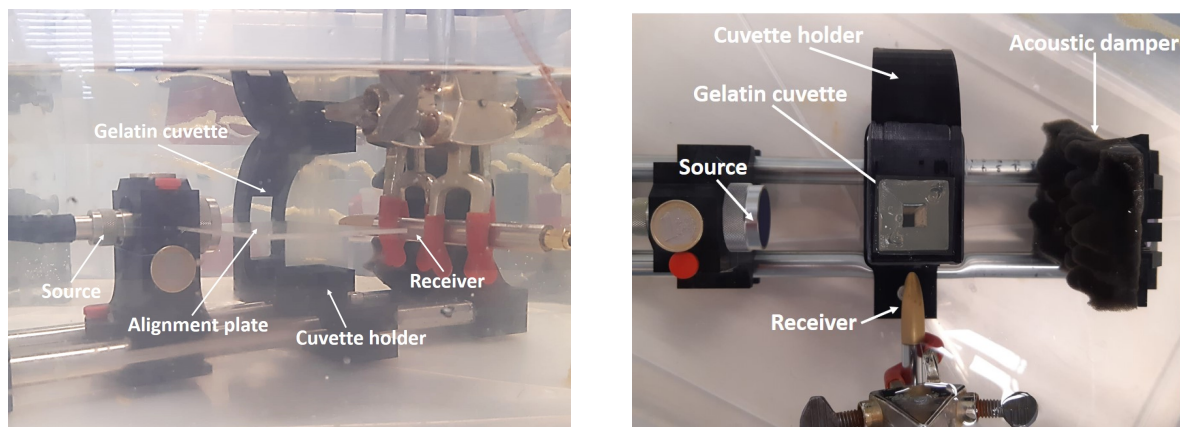
#### 159 II.A.1. Contrast agent fabrication and preparation

160 Endoskeletal antibubbles were produced as described by Poortinga<sup>6</sup> with some modifica-  
161 tions. The antibubbles were stabilized using pharmaceutical grade Aerosil<sup>®</sup> 972 Pharma  
162 hydrophobized silica particles (Evonik Industries AG, Essen, Germany). The aqueous cores  
163 were replaced by 2 vol% (sample 1) of hydrophobically modified Zano 10 Plus ZnO nanopar-  
164 ticles (Umicore, Brussels, Belgium). Reference bubbles containing no cores were produced  
165 in the same way but without adding core material. As compared to the procedure in<sup>6</sup>, the  
166 mixing speed of the high-shear mixer (IKA T18 Ultra Turrax equipped with an S18N-19G  
167 rotor-stator) was increased to 12,000 rotations per minute to produce smaller antibubbles  
168 with a size comparable to that of conventional UCAs.

169 All UCAs were maintained at room temperature before activation. The concentrations  
170 of investigated UCA dispersions were chosen in the low range, where a linear dependence of  
171 the scattered energy<sup>28,39,41,42</sup> and attenuation<sup>28,43</sup> on bubble concentration has been reported.  
172 The adopted concentration was in the order of  $10^5$  bubbles/mL for all studied UCAs, yielding  
173 a sufficient signal-to-noise ratio of the received signals. Preparation of reference bubble and  
174 antibubble dispersions was identical. 10 mg of dried material was diluted with 12 mL of  
175 saline in a vial. The resulting dispersions was manually gently agitated for 10 seconds, 0.35  
176 mL was taken out and diluted in 3.35 mL of saline, giving a concentration of 0.08 mg per 1  
177 mL. This corresponded to  $10^5$  bubbles/mL, based on the calculation of the overall gas volume  
178 corresponding to 0.08 mg of powder material and the average bubble volume. SonoVue<sup>™</sup>  
179 was prepared according to the manufacturer instructions. The vial was gently agitated, and  
180 0.4 mL of the dispersions was extracted right before the measurement and diluted to the  
181 concentration of 1  $\mu$ g per 1 mL which corresponds to  $8 \times 10^4$  bubbles/mL. For all UCAs the  
182 final dispersions was gently shaken manually for 10 seconds right before the measurement.

## 183 II.A.2. Experimental procedure

184 The center of the cuvette with UCA dispersions was always positioned a few millimeters  
 185 beyond the focal point of an US source (Fig. 3). A source holder and a cuvette holder  
 186 were fixed on a rail system, providing alignment of the source and the cuvette. The uti-  
 187 lized sources were all single-element focused US circular transducers with a diameter of 2.5  
 188 cm, and a focal distance of  $6.4 \pm 0.1$  cm. Transducers of type V302-SU-F, V304-SU-F and  
 189 V380-SU-F (Olympus Nederland B.V., Leiderdorp, the Netherlands), were excited at their  
 190 center frequencies of 1, 2.25 and 3.5 MHz, respectively. The omnidirectional secondary field  
 191 created by the UCAs was recorded with a 1.0 mm needle hydrophone (Precision Acoustics  
 192 Ltd., Dorchester, UK), oriented perpendicular to the source (Fig. 3). This is a typical  
 configuration of the source and the receiver, utilized for scatter measurements<sup>12,38,42,44</sup>.



193 Figure 3: The setup for scatter measurements. (a) Side view. (b) Top view.

194 Gelatin cuvettes were prepared to contain the contrast agents during the experiments.  
 195 Their advantage is a similar acoustic impedance to that of water and, therefore, low reflection.  
 196 For cuvette fabrication, a hollow form and a ceiling top were 3D printed. The black cubic  
 197 form was hollow, with inner dimensions of 12 by 3 by 3 cm. A lid was printed to seal the  
 198 top of the cuvette once the liquid gelatin mixture was inside. This lid had a long cubic  
 199 stick in the center with dimensions 10 by 1 by 1 cm. This construction shaped cubic gelatin  
 200 cuvettes with 1 cm thick sides, and a hollow cubic void (with the dimensions of the cubic  
 201 stick), where contrast material could be poured in. When preparing the gelatin mixture, 8  
 202 sheets of animal-based gelatin (Dr. Oetker, Amersfoort, The Netherlands) were diluted in  
 203 100 mL of water, corresponding to a concentration of 13 grams of gelatin per 100 mL. The

204 mixture was poured in the hollow form, smeared with vaseline from the inside. The form  
205 was sealed with the lid and put in the fridge.

206 Prior to the scatter measurements, the voltage amplitudes of the driving signals were  
207 identified for each transducer in order to generate MIs of 0.2 and 0.3. These mechanical  
208 indexes are often used in clinical practice since they do not induce either bubble bursting or  
209 damage to biological tissue<sup>34,35</sup>. Nevertheless, such signals are sufficiently strong to trigger  
210 nonlinear bubble oscillation. In the MI measurement, the gelatin cuvette was modified to  
211 position the hydrophone in the center of the cuvette. The generated pressures were recorded  
212 for various voltage amplitudes of the signals driving the source. The initial placement of the  
213 hydrophone in the center of the cuvette was visually aided, further adjustments were per-  
214 formed with the help of an oscilloscope, identifying the angular orientation of the hydrophone  
215 with the maximum signal amplitude.

216 Before the scatter measurement, the setup was submerged in a degassed water bath and  
217 left for a half an hour, allowing the gelatin phantom extracted from the fridge to reach room  
218 temperature. Two sides of the water tank, facing the source, were lined with foam to reduce  
219 possible reflections. The first measurement was always conducted for the reference liquid  
220 of saline. Additional acquisitions with a needle on the inside borders of the cuvette, were  
221 acquired to identify the region where the UCA signal was expected to originate. Further, the  
222 cuvette was emptied, the contrast-agent dispersions gently shaken and slowly injected in the  
223 cuvette. The UCA was shaken to ensure a homogeneous dispersion, i.e., with a homogeneous  
224 spatial distribution of bubbles/antibubbles, filling the whole inner cavity of the cuvette. The  
225 measurement was performed right after injection not to allow the larger bubbles with more  
226 gas to rise. Two driving voltages were used one after another, corresponding to  $MI = 0.2$  and  
227  $MI = 0.3$ , in an ascending order. The whole measurement lasted for a couple of seconds. This  
228 procedure was repeated 15 times for each UCA, with different batches of the contrast-agent  
229 dispersions being injected in the cuvette.

230 Labview (National Instruments Corp., Austin, TX, USA) was used to control the US  
231 acquisition of the acoustic response generated by UCAs. A 33220A arbitrary wave gen-  
232 erator (Agilent Technologies, Santa Clara, California, USA) was connected to a desktop  
233 and controlled by dedicated Labview software to generate the driving signals. The driving  
234 signals were transmitted to a 50-dB 2100L RF Power amplifier (Acquitek, Massy, France)

235 connected to the source transducer. The received signals were displayed on a TDS2014 oscil-  
 236 loscope (Tektronix U.K. Limited, Bracknell, UK) and were further sampled throughout an  
 237 NI-5122 (National Instruments Corp.) acquisition board which was connected back to the  
 238 desktop and controlled by the Labview software. Sinusoidal tone bursts with a rectangular  
 239 window, were transmitted by 3 sources driven at their center frequencies of 1, 2.25 and 3.5  
 240 MHz. A length of 20 cycles was chosen for 2.25 MHz and 3.5 MHz, and 10 cycles for 1 MHz.  
 241 These pulse lengths provided a sufficiently narrow bandwidth of the transmitted signals and,  
 242 therefore, allowed avoiding overlap between the harmonics in the received spectrum. The  
 243 silence period between the pulses was always set to 250 microseconds, chosen to prevent  
 244 interference of any possible reflection of the preceding pulse with the following pulse. A  
 245 total of 92-95 pulses was transmitted at every acquisition. The signals were recorded at a  
 246 sampling frequency of 25 MHz and stored for analysis.

### 247 II.A.3. Data analysis of scatter measurements

248 All data analysis was performed with MATLAB<sup>®</sup> (The MathWorks, Inc., Natick, MA, USA).  
 249 In the scatter measurement, the analyzed segment of the signal, generated by the UCAs was  
 250 identified manually, confirmed by the acquisitions with the needles inside the cuvette (Sec.  
 251 II.A.2). A window of 9 microseconds was chosen for the analysis, defined by the shortest  
 252 signal generated by the UCAs. The length of the time window was fixed for all sonicating  
 253 frequencies. For each acquisition, an average Fourier amplitude spectrum was calculated  
 254 based on 92 acquisitions, radiated by the UCAs, using Matlab's Fast Fourier Transform  
 255 function. A Hanning window was used in all cases to reduce spectral leakage<sup>45</sup>. The scatter  
 256 spectra were represented in two ways. First, using

$$257 \quad S(f) = 10 \log_{10} \left( \frac{A_{CA}(f)}{A_{sal}(f)} \right), \quad (1)$$

258 where  $A(f)_{CA}$  is the amplitude of the signal generated by the UCA at frequency  $f$  and  $A(f)_{sal}$   
 259 the amplitude of the signal at frequency  $f$  acquired with saline in the cuvette, representing  
 260 the noise level at that frequency<sup>23</sup>. In the second representation, the spectra were normalized  
 261 by the amplitude of the fundamental frequency  $A_{CA}(f_0)$  in these spectra, using

$$262 \quad S_n(f) = 10 \log_{10} \left( \frac{A_{CA}(f)}{A_{CA}(f_0)} \right). \quad (2)$$

263 For each medium studied, the responses of 15 acquisitions, calculated with Eqs 1 and 2, were  
264 averaged, and their standard deviation was assessed.

265 Equation 1 allows comparison of the UCA efficacy at the concentrations used. However,  
266 this concentration is significantly lower than that used in the clinic<sup>46,47</sup>. Since in the low  
267 concentration range all the generated harmonic amplitudes are proportional to the bubble  
268 concentration<sup>39,42</sup>, we normalized the UCA responses at all frequencies by the corresponding  
269 responses at the fundamental frequency, as shown in de Jong et al.<sup>30</sup>. Besides this, the  
270 scattered energy for every harmonic is also proportional to the squared bubble radius<sup>42</sup>.  
271 Therefore, it is hypothesized that this normalization reduces the influence of bubbles size  
272 and concentration on the scattered spectra.

273 Assessment of the significance of the differences between the higher harmonics of the  
274 UCAs was performed with the two-tailed Student's t-test, assuming a Gaussian distribution  
275 of the higher harmonic amplitudes among the 15 acquisitions. A p-value below 0.05 is  
276 considered to indicate a statistically significant difference between the distributions.

## 277 II.B. Attenuation measurements

278 The attenuation measurement was performed with a transmission setting (Fig. 4). The same  
279 source transducers as for the scatter measurement (Sec. II.A.) were employed, resulting in  
280 attenuation coefficients at 3 frequencies for all studied UCAs. The sources, the receivers and  
281 the cuvette with UCAs were fixed on the same rail system as for the scatter measurement.  
282 The center of the cuvette was positioned in the focal region of the sources. The opening in  
283 the gelatin cuvette containing UCA was 1.6-cm wide, ensuring that the whole beam passed  
284 through the studied dispersions. The length of the cuvette, corresponding to the path in the  
285 UCA dispersion, was 1 cm. Varying greatly among other experimental studies, from 2 cm to  
286 8 cm,<sup>38,48,49,50</sup>, this cuvette length was chosen to ensure a sufficient signal-to-noise ratio after  
287 propagation through all studied UCAs at all frequencies. The receiver was fixed in a holder  
288 located 85 mm away from the cuvette (Fig. 4). A plane piston V306 transducer (Panametrics-  
289 NDT, Olympus NDT Inc., Waltham, MA, USA), centered at 2.25 MHz was used as the  
290 receiver for measurements at 1 and 2.25 MHz, and a plane piston V309 (Panametrics-NDT,  
291 Olympus NDT Inc., Waltham, MA, USA) was used for 3.5 MHz. The same system and  
292 control software was used for the attenuation measurement (Sec. II.A.2.), transmitting 20-

293 cycle tone bursts for all frequencies. For every source, transmitted pressure amplitudes were  
 294 below 60 kPa, measured in the center of the cuvette by the hydrophone, as for the scatter  
 295 measurement (Sec. II.A.2). At such low pressures, the bubble oscillation is **mostly** linear,  
 296 as demonstrated in (Kudo et al., 2020)<sup>7</sup> for antibubbles **and reference bubbles**. SonoVue<sup>TM</sup>,  
 297 **on the other hand**, exhibited an initiation of 2nd harmonic growth at pressures of 24 to 50  
 298 kPa<sup>30,51</sup>, depending on the transmit frequency. Therefore, a preliminary experiment was  
 299 **conducted**, assessing the higher harmonic amplitudes for the chosen settings, demonstrating  
 300 **the higher harmonics to be below 5%** of the fundamental signal. This way, it was concluded  
 301 **that the chosen settings primarily corresponded to the linear regime of bubble oscillation**.  
 302 Contrast-agent dispersions were prepared as for the scattering measurement (Sec. II.A.1).  
 They were injected in a gelatin cuvette right before the measurement. Attenuation was

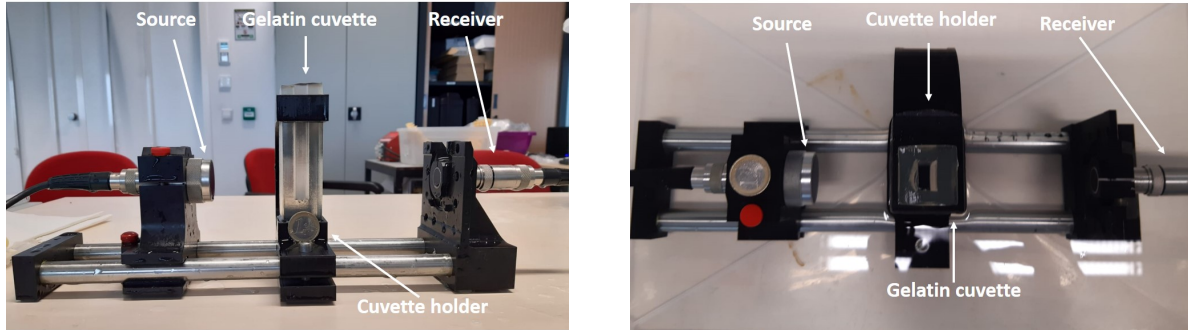


Figure 4: The setup for attenuation measurements. (a) Side view of the setup taken out of  
 303 the water bath. (b) Top view.

304 estimated based on two measurements: when the cuvette contained 7 mL of saline and 7  
 305 mL of UCA. The Fast Fourier Transform was performed on all the received pulses in the  
 306 acquisitions and the average amplitude at the fundamental frequency was extracted for saline  
 307  $A_{\text{sal}}$  and UCA  $A_{\text{CA}}$ . The attenuation coefficient was computed using

$$308 \quad \alpha(f) = \frac{20}{d} \log_{10} \left( \frac{TA_{\text{sal}}(f)}{A_{\text{CA}}(f)} \right), \quad (3)$$

309 where  $d$  is the length of the US path in the UCA medium defined by the inner dimensions of  
 310 the cuvette and  $T$  is the transmit coefficient<sup>38,49</sup>. For every UCA, 15 acquisitions were per-  
 311 formed, yielding 15 values of the attenuation coefficient. The mean and standard deviation  
 312 among these acquisitions were assessed.

313 In our measurement in Eq. 3,  $d = 1$  cm and  $T$  was approximated to 1, neglecting all  
 314 reflection losses and possible acoustic impedance differences of UCAs with respect to water.

315 In an experiment designed to verify this assumption for our gelatin cuvettes, it was identified  
316 that the amplitude of the transmitted pulse decreased by 1% only per 1 cm of the path in  
317 gelatin. These losses include reflection loss (defined by the difference in acoustic impedance)  
318 and attenuation. As for UCAs, the density was assumed identical to that of water due to  
319 the low concentration of bubbles used. The arrival times of the pulses transmitted through  
320 UCAs were compared to that in water. A maximum delay among all UCAs corresponded to  
321 0.6 microseconds, indicating a maximum difference of 8 % in the speed of sound compared to  
322 water. For the three investigated frequencies, an attenuation measurement was conducted  
323 for corn oil, utilizing the same setup and making the same assumptions. The attenuation  
324 coefficients were in agreement with literature values<sup>52</sup>, within a  $\pm 0.1$  dB/cm error.

325 To verify the measured attenuation values, another attenuation measurement was con-  
326 ducted with a different set up for 3.5 MHz, at the same acoustic pressure amplitude as  
327 for the through-transmission measurement, corresponding to  $MI = 0.03$ . 20-cycle pulses  
328 were transmitted, with a Gaussian window. An L11-4v linear array probe, controlled by a  
329 Verasonics US system (Vantage 128, Verasonics Inc.), was utilized to construct echo-mode  
330 videos, consisting of 100 frames. The image gain was set constant throughout depth and  
331 no log compression was performed, therefore, the graylevels of the videos represented the  
332 envelopes of the signals. The probe was positioned to provide normal incidence of the son-  
333 icating beam on the cuvette, while an aluminium plate behind the cuvette served as the  
334 reflector, as in<sup>53</sup>. A reference measurement with saline in the cuvette was performed, where  
335  $A_{\text{sal}}$  was the grayvalue of the aluminium plate (Eq. 3), averaged over the 100 frames. Then  
336 the saline was taken out with a syringe and the UCA suspension was injected in the cuvette,  
337 resulting in a mean graylevel of the aluminium plate  $A_{\text{CA}}$ . The difference in the grayscale  
338 intensity of the aluminium plate in these two measurements allows to compute the attenu-  
339 ation coefficient (Eq. 3), accounting for the longer path through the UCA dispersion due  
340 to forward and backward directions. For all UCAs, the attenuation coefficient of 6 or 7  
341 analogous dispersions was measured.

342 Besides this, the ratio of the pressures backscattered by the UCA suspensions to the  
343 transmitted pressure amplitudes was estimated for 3.5 MHz. For this estimation, the cu-  
344 vette was removed from the acoustic path. The graylevel intensity of the aluminium plate  
345 divided by the reflection coefficient of the water-aluminium interface represented the sonicat-  
346 ing amplitude  $A_{\text{transmit}}$ . The mean graylevel inside the cuvette represented the backscattered

347 energy  $A_{\text{backsc}}$ . The ratio was computed as

$$348 \quad S_{\text{lin}}(f) = \frac{A_{\text{backsc}}(f)}{A_{\text{transmit}}(f)} \times 100\%. \quad (4)$$

349  $S_{\text{lin}}$  represents the linear scatter at the fundamental frequency, since higher harmonic gener-  
 350 ation at these pressures was demonstrated to be negligible for antibubbles, reference bubbles  
 351 and SonoVue<sup>TM</sup> 7,42,44.

### 352 II.C. Dynamic contrast-enhanced ultrasound measurement

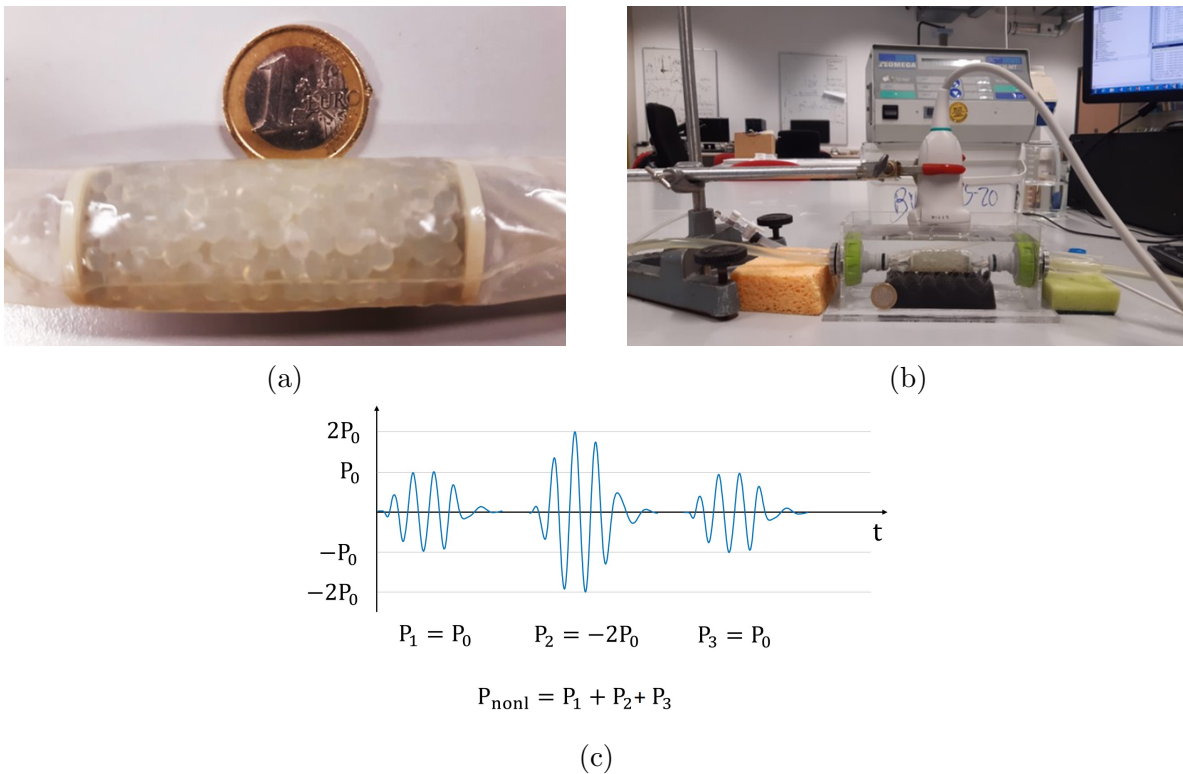


Figure 5: The setup for the dynamic contrast-enhanced ultrasound measurement. (a) A close-up view of a vascular phantom made of beads. (b) The probe is mounted on top of the vascular phantom, in a water bath. (c) The utilized pulse scheme, where three pulses were transmitted ( $P_1$ ,  $P_2$ , and  $P_3$ ) to form a DCE-US clip, reflecting the intensity of the nonlinear signal  $P_{\text{nonl}}$ .

353 To investigate the efficacy of UCAs in a near to clinical setting, a DCE-US measurement  
 354 was performed. In this measurement, the UCAs were separately injected into a perfusion  
 355 system, flowing through a porous phantom that mimicked a microvascular network. De-  
 356 gassed water flow through the phantom was supplied with an FPU5-MT peristaltic pump  
 357 (Omega Engineering Ltd., Manchester, UK) at a rate of 36 mL/min. The utilized flow was



358 in the range of expected physiological values, ranging from  $10^{-7}$  mL/min for capillaries<sup>54</sup>  
359 to  $10^3$  mL/min for large arteries<sup>54,55</sup>. The porous phantom (Fig. 5a) was built by packing  
360 alginate beads with a diameter of 3.1 mm in a polyurethane tube, whose shape was fixed by  
361 two circular nets at the two sides of the phantoms. The phantom was gently squeezed and  
362 shaken after packing to achieve a more homogeneous structure<sup>40</sup>. The spaces between the  
363 beads simulated a microvascular network with porosity of 43%. Since the phantom consisted  
364 of identical beads, the simulated microvascular network did not exhibit the vessel/capillary  
365 topology typical for biological tissue<sup>54,56</sup>. The water resistant alginate beads did not permit  
366 simulating tissue-water exchange observed in biological tissue<sup>57</sup>. This way, the phantom pro-  
367 vided a simplified model of a microvascular network. The phantom used in the experiments  
368 was about 4.5 cm long, comparable to the length of the utilized US transducer, and 2 cm  
369 in diameter. Before the experiment, the phantom was submerged in a water bath and con-  
370 nected to the input and output flow paths (Fig. 5b). A linear array L11-4v probe, controlled  
371 by a Verasonics US system, was mounted above the phantom. DCE-US plane wave imaging  
372 was performed in contrast-specific mode following the manual injection of a UCA bolus into  
373 the flow stream towards the vascular phantom. The utilized pulse scheme is illustrated in  
374 Fig. 5c, consisting of one high-amplitude pulse and two pulses, twice as low in amplitude  
375 and shifted in phase by  $180^\circ$ . The high-amplitude pulse pressure was 370 kPa, corresponding  
376 to  $MI = 0.2$  (the probe was calibrated with the same hydrophone). The transmitted pulses  
377 consisted of 3 cycles at 3.5 MHz, granting sufficient resolution for visualization of the beads  
378 composing the phantom. The contrast-specific mode was a combination of pulse inversion  
379 and amplitude modulation schemes, since it was shown to be the most sensitive imaging  
380 strategy to microbubble nonlinearities<sup>58</sup>.

381 When injecting the contrast-agent bolus, we aimed to have the same concentrations at  
382 the peak of the time-intensity curves (TICs) as in the static measurement. A few preliminary  
383 measurements were conducted where 1 mL of reference bubble and antibubble dispersions  
384 (0.5 mg/mL) was injected. The water volume where the UCA was diluted<sup>2,3</sup> before its arrival  
385 to the middle of the vascular phantom was assessed with the measured TICs in the middle  
386 of the phantom. A simple triangular model<sup>59,60</sup> was used to correlate the concentration  
387 at the peak of the TIC and the identified mixing volume. For SonoVue<sup>TM</sup>, two greater  
388 concentrations were also used. Since the SonoVue<sup>TM</sup> bubbles are smaller, greater number  
389 densities were used to reach a volume fraction comparable to that in the reference and

antibubble boluses. In these cases the concentration of SonoVue<sup>TM</sup> at the peak of the TIC was estimated to be 10 and 30 times greater than the concentration used in the static measurement.

For every UCA 4 DCE-US acquisitions were performed. For every acquisition, a 1-mL bolus with the calculated concentrations was injected. 40-second dynamic contrast-enhanced US clips recorded the flow through the porous phantom including the complete wash-in and wash-out. The TICs were extracted from the middle of the phantom (Fig. 5a) and compared, with the aim to identify the UCA producing the highest peak signal.

### III. Results

#### III.A. Scattering

The average spectra of the signals generated by UCAs, normalized to the saline spectrum are presented in Fig. 6. The frequencies of the sonicating signals are stated above the plots. The thick vertical straight lines on the plots indicate this sonicating frequency and, therefore, the fundamental component of the signal scattered by UCAs. The thinner lines indicate integers of the fundamental frequency, representing the scattered higher harmonics. The error bars next to these lines demonstrate the mean and the standard deviation of the higher harmonic amplitudes among the 15 acquisitions for antibubbles (to the left of the harmonic line, in blue), reference bubbles (on the harmonic line, in red) and SonoVue<sup>TM</sup> (to the right of the harmonic line, in magenta). For the top plots, demonstrating the UCA response to sonication at an MI of 0.2, for 1 MHz and 2.25 MHz the nonlinear responses of antibubbles and reference bubbles are equivalent: the mean higher harmonic amplitudes differ no more than by 2 dB, with no significant differences in the higher harmonic distributions ( $p > 0.05$ ). For 3.5 MHz, the antibubbles scatter a 2nd harmonic 2 dB greater than the reference bubbles, with a significant ( $p < 0.001$ ) difference in the distributions. The 3rd harmonic content is equivalent. For SonoVue<sup>TM</sup>, at 1 MHz, all higher harmonics are up to 2 dBs weaker than those of antibubbles with a significant difference in the higher harmonic distributions ( $p < 0.05$ ). For 2.25 MHz and 3.5 MHz, SonoVue<sup>TM</sup> exhibits an analogous nonlinear response to antibubbles, with barely a difference in higher harmonic amplitudes and complete or great overlap of the confidence intervals ( $p > 0.05$ ). For an MI of 0.3, all higher

419 harmonics generated by antibubbles are significantly ( $p < 0.01$ ) greater than for the reference  
 420 bubbles, at all the sonicating frequencies. In comparison to SonoVue™, at 1 MHz the higher  
 421 harmonic amplitudes of antibubbles are 2 to 4 dB greater ( $p < 0.001$ ). At 2.25 MHz, the non-  
 422 linear responses are equivalent ( $p > 0.05$ ), while for 3.5 MHz the 2nd and 3rd harmonic of  
 423 antibubbles are significantly ( $p < 0.001$ ) greater (up to 2 dB) than those of SonoVue™.

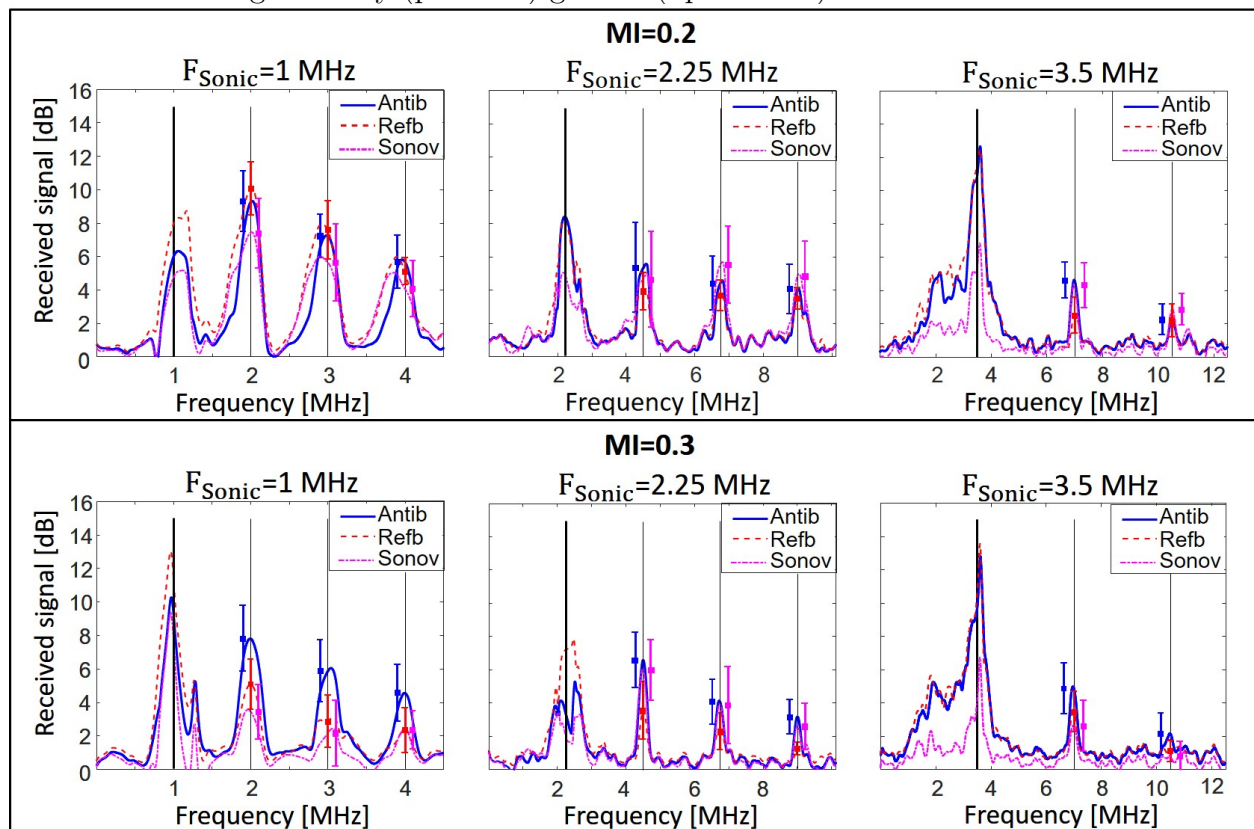


Figure 6: Mean spectra of the signals generated by antibubbles (Antib), reference bubbles (Refb) and SonoVue™ (Sonov) at frequencies of 1, 2.25 and 3.5 MHz for MIs of 0.2 (top) and 0.3 (bottom). The amplitude of the responses is presented in dB, normalized with respect to the responses in a reference acquisition with saline in the cuvette. The thick vertical lines indicate the fundamental frequency, while the thin vertical lines indicate higher harmonics. The error bars represent the standard deviations of the higher harmonic amplitudes.

424 The spectra normalized to their corresponding fundamental signals are shown in Fig.  
 425 7. Theoretical analysis predicts that all the harmonic amplitudes scattered by a UCA dis-  
 426 persion are proportional to the bubble concentration, in the low concentration range, and  
 427 the bubble radius<sup>11,39,42</sup>. Normalizing the spectrum to the fundamental harmonic amplitude  
 428 is hypothesized to mitigate to some extent the impact of the different bubble sizes and  
 429 concentrations. This way, the provided normalized plots facilitate comparing the nonlinear

behavior of the investigated bubbles/antibubbles. Analysis of the scatter spectra at pres-

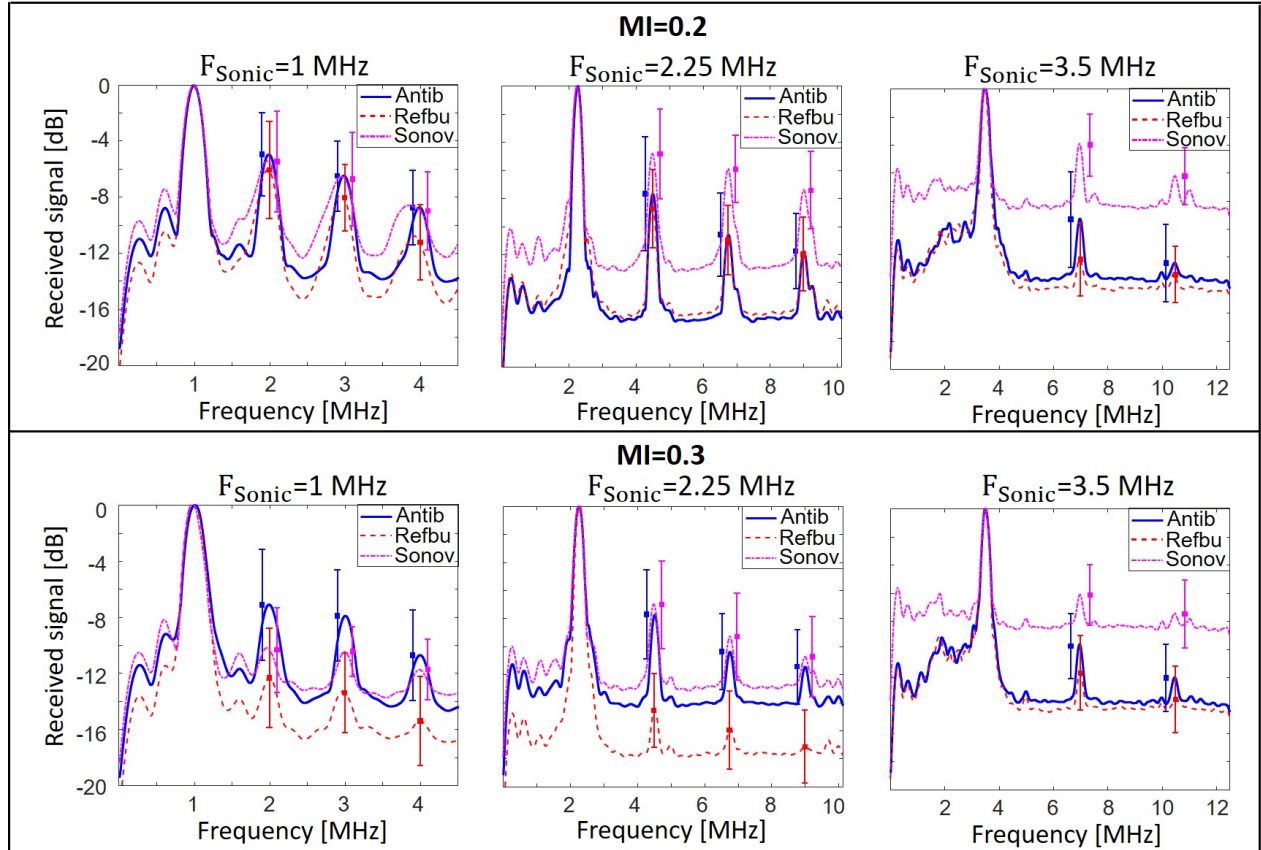


Figure 7: Spectra of the signals generated by UCAs at frequencies of 1, 2.25 and 3.5 MHz for MIs of 0.2 and 0.3. The amplitude of the responses is presented in dB, normalized with respect to the fundamental component in these responses.

430

431 sures corresponding to an  $MI = 0.2$  follows below. At 1 MHz, antibubbles generated mean  
 432 higher harmonic amplitudes equivalent to those of SonoVue<sup>TM</sup>, with nearly complete over-  
 433 lap of the confidence intervals ( $p > 0.05$ ). The mean higher harmonic amplitudes of reference  
 434 bubbles are somewhat lower than those of antibubbles, with the greatest significant ( $p < 0.01$ )  
 435 difference of 3 dB in the 4th harmonic. At 2.25 MHz, higher harmonics of antibubbles are  
 436 up to 5 dB weaker (3rd harmonic) than those of SonoVue<sup>TM</sup>, with a significant difference  
 437 between the harmonic distributions ( $p < 0.05$ ), and equivalent to reference bubbles ( $p > 0.05$ ),  
 438 with the antibubble signal up to 1 dB greater than that of reference bubbles. At 3.5 MHz,  
 439 antibubble higher harmonics are significantly ( $p < 0.001$ ), up to 6 dB weaker than those of  
 440 SonoVue<sup>TM</sup>. At the same time, they are up to 3 dB greater than those of reference bubbles  
 441 with a significant difference between the scattered higher harmonics ( $p < 0.01$ ).

442 Analysis of the scatter responses at pressures corresponding to an  $MI = 0.3$  follows  
443 below. For 1 MHz, antibubble higher harmonics are up to 3 dB greater ( $p < 0.05$ ) than those  
444 of SonoVue<sup>TM</sup> and up to 6 dB greater than those of reference bubbles ( $p < 0.001$ ). At 2.25  
445 MHz, antibubble higher harmonics are equivalent to those of SonoVue<sup>TM</sup>, with a maximum  
446 difference of 1 dB and a p-value above 0.05. Antibubble higher harmonics are up to 7 dB  
447 greater than those of reference bubbles, with no overlap of the confidence intervals ( $p < 0.001$ ).  
448 At 3.5 MHz, antibubbles scatter higher harmonics that are significantly different from those  
449 of reference bubbles and SonoVue<sup>TM</sup>: they are up to 2 dB greater than those of reference  
450 bubbles ( $p < 0.05$ ) and up to 5 dB weaker than those of SonoVue<sup>TM</sup> ( $p < 0.001$ ).

451 Comparing plots at  $MI = 0.2$  and  $MI = 0.3$ , in several cases the higher harmonic  
452 amplitudes decrease for higher pressures, compared to lower pressures. At 1 MHz, we observe  
453 this for all contrast agents ( $p < 0.05$ ). For 2.25 MHz this is observed for SonoVue<sup>TM</sup> and  
454 reference bubbles ( $p < 0.05$ ), while the signal scattered by antibubbles is equivalent for both  
455 sonicating pressures ( $p > 0.05$ ). At 3.5 MHz, SonoVue<sup>TM</sup>'s higher harmonics decrease for the  
456 higher pressure ( $p < 0.05$ ), while those of antibubbles and reference bubbles stay equivalent  
457 ( $p > 0.05$ ).

### 458 III.B. Attenuation

459 Figure 8 illustrates the mean attenuation of antibubbles, reference bubbles and SonoVue<sup>TM</sup>,  
460 with the corresponding standard deviations. For all frequencies, the mean attenuation coef-  
461 ficient is greater for antibubbles, compared to reference bubbles and SonoVue<sup>TM</sup>. At 1 MHz,  
462 antibubbles' attenuation coefficient is slightly higher than that of the reference bubbles, with  
463 a mean and significant difference of 1 dB/cm ( $p < 0.05$ ). For other measurements, all the dif-  
464 ferences in UCA attenuation are significant as well ( $p < 0.001$ ). At 1 MHz, the antibubble  
465 mean attenuation coefficient is 8.4 dB/cm greater than that of SonoVue<sup>TM</sup>. For 2.25 MHz, it  
466 is 6.7 dB/cm greater than that of reference bubbles and 9.1 dB/cm than that of SonoVue<sup>TM</sup>.  
467 At 3.5 MHz, it is 2.6 dB/cm greater than that of reference bubbles and 3.4 dB/cm greater than  
468 of SonoVue<sup>TM</sup>. The antibubbles attenuation coefficients are 8.7 dB/cm, 9.7 dB/cm and 4.4  
469 dB/cm for 1 MHz, 2.25 MHz and 3.5 MHz, respectively.

470 The attenuation measurement conducted in echo-mode with the Verasonics system  
471 yielded attenuation values of 2.8 dB/cm, 1.1 dB/cm and 0.4 dB/cm for antibubbles, ref-

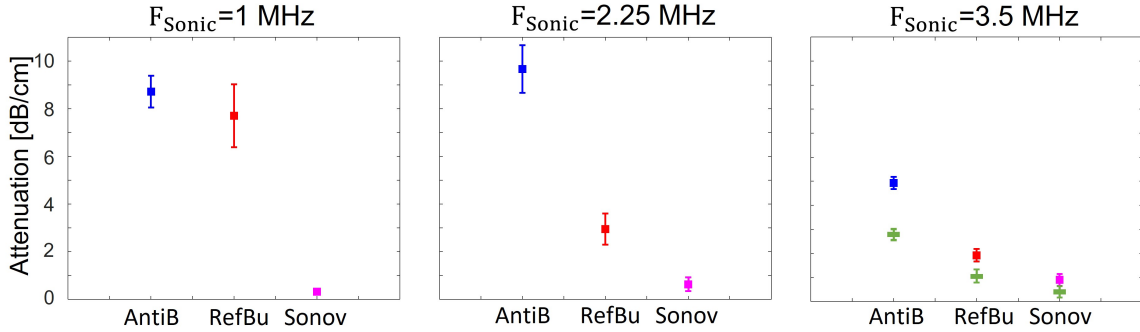


Figure 8: Attenuation coefficients measured for antibubbles (AntiB), reference bubbles (Refb) and SonoVue<sup>TM</sup> (Sonov) at sonicating frequencies of 1, 2.25 and 3.5 MHz (left to right). The square symbols indicate the mean attenuation coefficients measured with the piston source and receiver (Fig. 4). The rectangular (green) symbols indicate the mean attenuation measured in echo-mode with the Verasonics probe for 3.5 MHz.

472 reference bubbles and SonoVue<sup>TM</sup>, respectively, illustrated with star-symbols in Fig. 8. The  
 473 portion of the backscattered pressures  $S_{lin}$  (Eq. 4) constituted 4%, 6% and 2% of the trans-  
 474 mitted pressures for antibubbles, reference bubbles and SonoVue<sup>TM</sup>, respectively.

### 475 III.C. Dynamic contrast-enhanced ultrasound

476 Figures 9a-9d demonstrate the maximum intensity projections of the DCE-US clips record-  
 477 ing antibubble, reference bubble and SonoVue<sup>TM</sup> passage through the employed porous phan-  
 478 tom. These images simulate potential clinical images of tissue, when imaging a UCA bolus  
 479 passage in contrast-specific mode at pressures inducing nonlinear bubble oscillation. Fig-  
 480 ure 10 demonstrates the mean linearized TICs of the UCAs, normalized to the maximum  
 481 mean peak intensity among the UCAs. From the measured TICs, one can observe that  
 482 antibubbles generate a peak nonlinear signal 31% greater than that of the reference bubbles,  
 483 224% greater than that of SonoVue<sup>TM</sup> at the concentration studied in the static measure-  
 484 ments, 53% greater than SonoVue<sup>TM</sup> at 10 times the concentration studied in the static  
 485 measurements and 23% lower than that of SonoVue<sup>TM</sup> at the highest studied concentration.

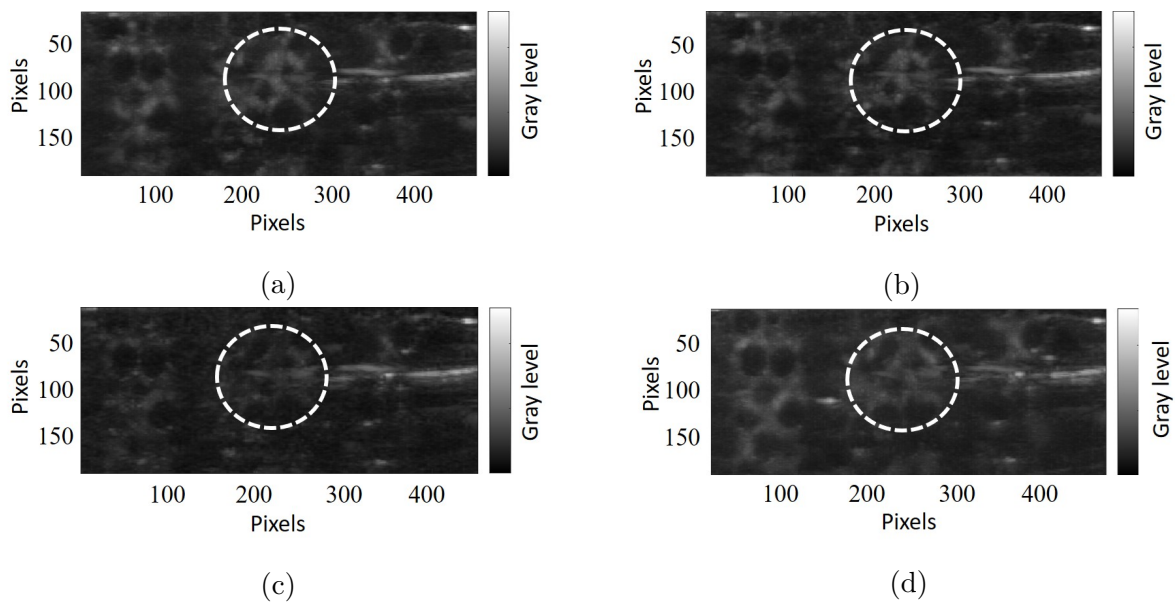


Figure 9: Maximum intensity projection based on the DCE-US recordings of UCAs passing through the porous phantom. The white contour indicates the region of interest where the TICs were extracted. (a) Antibubbles. (b) Reference bubbles. (c) SonoVue<sup>TM</sup> with a peak concentration as in the static measurement. (d) SonoVue<sup>TM</sup> with a peak concentration 30 times higher than in the static measurement.

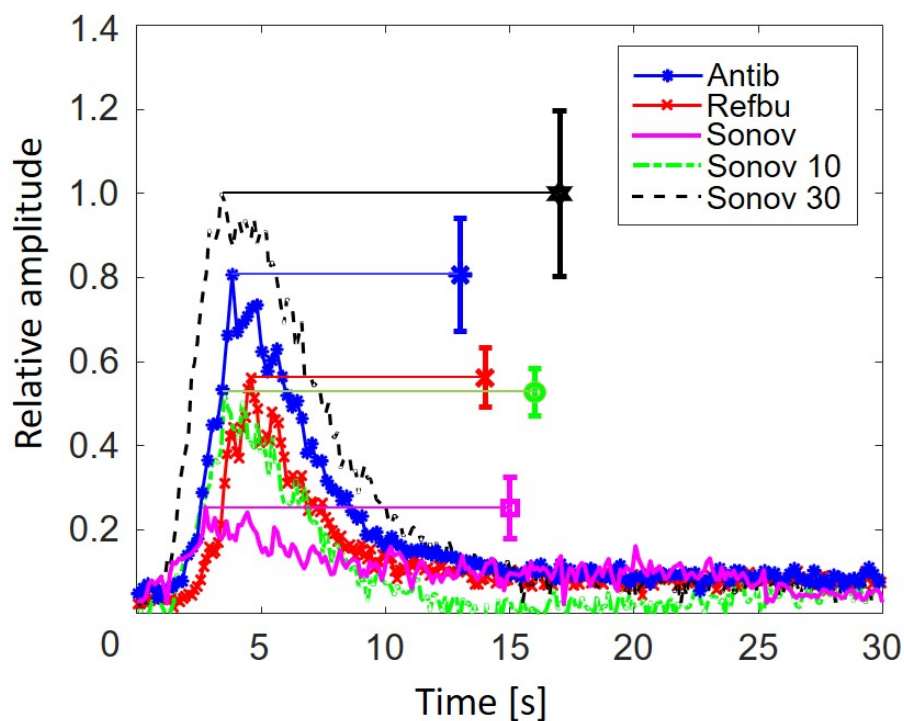


Figure 10: Linearized TICs of the middle region of the vascular phantom, averaged among 4 acquisitions for all studied dispersions. The peak amplitude for antibubbles, reference bubbles and SonoVue<sup>TM</sup> is generated by the same concentration of contrast agents as in the static measurement. The peak concentrations of Sonov10 and Sonov30 are 10 and 30 times higher than that in the static measurement. The error bars illustrate the standard deviation at the point of maximum intensity of the averaged curves.



## IV. Discussion

The scatter spectra normalized to the saline spectrum (Fig. 6) show antibubble higher harmonics to be equivalent or slightly greater, compared to reference bubbles and SonoVue<sup>TM</sup> in the studied frequency range. On the scatter spectra of SonoVue<sup>TM</sup> across all frequencies, we can not appreciate the expected growth in harmonic amplitude for the frequencies of 2.25 MHz and 3.5 MHz, close to its reported resonance frequency<sup>30</sup>, in comparison to 1 MHz. This underlines that the scatter plots for separate sonicating frequencies do not demonstrate the frequency dependence of the UCA response. The sonicating field is different for every studied frequency, with different dimensions of the focal spot for each source.

For every sonicating frequency, comparing the spectra at  $MI = 0.2$  and  $MI = 0.3$ , we could not appreciate any marked growth of the nonlinear components of the scattered signals with increasing pressure amplitude. Markedly, at frequencies of 1 MHz and 3.5 MHz, at  $MI = 0.3$ , unlike at  $MI = 0.2$ , antibubbles scatter a higher nonlinear signal, compared to both other UCAs ( $p < 0.01$ ). The spectrum corresponding to 1 MHz and  $MI = 0.3$  exhibits an increase of broadband noise between the 2nd and 3rd harmonic, compared to  $MI = 0.2$ , possibly indicating the onset of bubble cavitation<sup>61,62</sup>. It is also possible that the lower harmonic amplitudes at  $MI = 0.3$  are attributed to the rise of larger bubbles to the surface, since the scatter acquisitions at  $MI = 0.3$  were performed 2-5 seconds after those at  $MI = 0.2$ . Interestingly, antibubbles, the heaviest bubbles, exhibit the lowest difference in harmonic amplitudes for both MIs, while SonoVue<sup>TM</sup>, the lightest bubbles, exhibit the greatest difference. This indicates that for future characterization, the acquisition at all studied pressures should be performed right after injection of the contrast agents in the cuvette. Alternatively, a thickener can be added to increase the viscosity of the saline, slowing down the rise of larger bubbles to the surface of the dispersion, or a magnetic stirrer could be utilized to keep the dispersion uniform, as in<sup>48</sup>.

The scatter spectra, normalized to the corresponding fundamental signal in the spectrum (Fig. 7), shows antibubble higher harmonics to be equivalent or up to 3 dB greater than those of reference bubbles. At frequencies of 2.25 MHz and 3.5 MHz, and pressures corresponding to  $MI = 0.2$ , SonoVue<sup>TM</sup> scattered the greatest higher harmonic amplitudes among the studied UCAs. This may indicate that, in the given experimental configuration, SonoVue<sup>TM</sup> has a greater capacity to scatter higher harmonics, compared to antibubbles

517 and reference bubbles. At equivalent bubble size and bubble concentration, SonoVue<sup>TM</sup> may  
518 generate a stronger nonlinear signal. This **might not have been** appreciated on Fig. 6 due  
519 to the smaller size of SonoVue<sup>TM</sup> bubbles or a somewhat lower concentration. **On the other**  
520 **hand, the provided normalization cannot fully compensate for the influence of the size distri-**  
521 **bution, as the energy scattered by a certain UCA dispersion is the energy integrated over the**  
522 **bubble size distribution through a complex nonlinear process. Experiments involving other**  
523 **bubble/antibubble size distributions are needed to confirm the observations in Fig. 7.”**

524 The attenuation measurement is an important indicator of UCA efficacy<sup>28</sup> since lower  
525 attenuation allows avoiding shadowing and imaging at further depth. Endoskeletal antibub-  
526 bles exhibit the greatest attenuation among the studied UCAs. Given that the attenua-  
527 tion coefficient of most studied dispersions of clinically-approved UCAs does not exceed 4.5  
528 dB/cm in the whole diagnostic frequency range<sup>29,44,63,64</sup>, and that most soft tissue types  
529 have an attenuation coefficient below 0.5 dB/(cm MHz)<sup>65,66</sup>, endoskeletal antibubbles ex-  
530 hibit remarkably high attenuation at 1 and 2.25 MHz. The high attenuation of antibubbles  
531 may be caused by the endoskeleton that may add a viscous behavior to the inner gas phase.  
532 Alternatively, the hydrophobic ZnO particles forming the endoskeleton were observed to be  
533 surrounded by a thin gaseous layer<sup>67</sup>. These tiny air pockets are acoustically active at low  
534 acoustic amplitudes, absorbing acoustic energy and cavitating<sup>67</sup>.

535 The attenuation measurement at 3.5 MHz, conducted with a Verasonics probe in  
536 echo-mode, yielded somewhat lower attenuation values for all UCAs than the through-  
537 transmission measurement with piston transducers. However, both measurements point out  
538 the same qualitative differences among UCAs. The discrepancy in the measurement results  
539 may be due to different pulse shapes: in the through-transmission acquisition a rectangular  
540 pulse was utilized, while a Gaussian pulse was transmitted in the echo-mode measurement.

541 The attenuation measurement is independent of the source pressure field<sup>30</sup>. The fre-  
542 quency of maximal attenuation of UCAs indicates the resonance frequency of the bubble  
543 population<sup>30,44</sup>. At this frequency, the bubbles transfer a greater portion of energy to higher  
544 harmonics. A resonance frequency close to 3.5 MHz is in line with studies that report a  
545 resonance frequency close to 3 MHz for SonoVue<sup>TM</sup><sup>30</sup>. Based on the attenuation measure-  
546 ments, the resonance frequency of reference bubbles is hypothesized to be close to 1 MHz, the  
547 frequency of maximum attenuation. Following the same reasoning, the resonance frequency

548 of antibubbles is hypothesized to be between 1 and 2.25 MHz, closer to 2.25 MHz. This  
549 is in line with a smaller size of antibubbles compared to the largest reference bubbles<sup>29,30</sup>.  
550 The presence of an incompressible core also increases the resonance frequency of a bubble<sup>7</sup>.  
551 However, it must be noted that the sonicating pressures differed for the studied frequencies  
552 and an additional measurement with equivalent pressures is advisable for future work.

553 At low acoustic pressures, where mainly linear low-amplitude bubble oscillation takes  
554 place<sup>7,42,44</sup>, endoskeletal antibubbles backscatter less energy than reference bubbles and more  
555 than SonoVue<sup>TM</sup> at the studied concentration, expressed in  $S_{lin}$  (Eq. 4). It is theoretically  
556 predicted that the backscattered energy is proportional to the gas volume in the UCA  
557 dispersions<sup>11,29,42</sup>. The same weight of dried contrast material was diluted in saline for  
558 antibubbles and reference bubbles, whereas antibubbles contain an endoskeleton and solid  
559 cores. This may have resulted in a greater number of reference bubbles than antibubbles,  
560 as shown in Fig. 2 (81 antibubbles versus 101 reference bubbles). At the same time, the  
561 reference bubble dispersion contains a small percent of reference bubbles almost twice as large  
562 as the largest antibubbles (Fig. 2). These bubbles have a greater scattering cross-section<sup>11,42</sup>.  
563 The SonoVue<sup>TM</sup> dispersion clearly contains a smaller gas volume with a comparable number  
564 of much smaller bubbles (Fig. 1).

565 The linearized TICs of the DCE-US acquisition exhibited periodic fluctuations (Fig.  
566 10). These can be attributed to the **pulsatile** flow of the utilized **peristaltic** pump and to  
567 reverberation between the surfaces of the probe and the porous phantom. The TICs showed  
568 antibubbles to backscatter a nonlinear signal 31% greater than that of the reference bubbles,  
569 224% greater than that of SonoVue<sup>TM</sup> at the concentration studied in the static measure-  
570 ments. This difference in the scattered signal is not present in the scatter measurement at  
571 the corresponding MI of 0.2, where antibubbles and SonoVue<sup>TM</sup> generate equivalent higher  
572 harmonics (Fig. 6). This finding may indicate that the scatter measurement was masked  
573 by the high attenuation of antibubbles surrounding the focal spot. Previous work<sup>23</sup> and  
574 preliminary work support this hypothesis. In preliminary scatter experiments (unpublished  
575 data), increasing the concentration of antibubbles and reference bubbles in homogeneous  
576 dispersions augmented the scattered nonlinear signal. However, the signal growth with con-  
577 centration was greater for reference bubbles than for antibubbles. This way, the difference  
578 between the amplitudes of the scattered nonlinear signal of reference bubbles and antibub-  
579 bles decreased with growing concentration. At the same time, in previous work<sup>23</sup>, a small

580 quantity of antibubbles at a concentration 100 times greater than that in the studied homo-  
 581 geneous dispersions, injected in the very center of the cuvette filled with saline (the location  
 582 of the peak pressure), generated a 2nd harmonic 10 dB greater than that generated by refer-  
 583 ence bubbles in the same setting. These findings support the conclusion that, in our scatter  
 584 measurement configuration, where homogeneous dispersions were used and the US field was  
 585 focused, attenuation affected the scatter measurement: the advantage of antibubbles over  
 586 reference and SonoVue™ bubbles in Fig. 6 and Fig. 7 was masked proportionally to the  
 587 their attenuation. Since this evidence is indirect, additional experiments, imaging the fun-  
 588 damental pressure field and the generated 2nd harmonic in the DCE-US setting would help  
 589 clarify whether the affect of attenuation was negligible on the generated and received 2nd  
 590 harmonic signal. Scatter measurements in a wider/narrower cuvette may identify what role  
 591 attenuation played in the scatter measurement.

592 At concentrations 10 and 30 times higher than that utilized in the scatter measurement,  
 593 the nonlinear response of SonoVue™ grows, and at the highest SonoVue™ concentration  
 594 the antibubble response is 23% lower than that of SonoVue™. It is important to note that  
 595 SonoVue™'s resonance frequency is close to 3 MHz, while antibubbles have been shown to  
 596 have a resonance frequency between 1 MHz and 2.25 MHz. Therefore, at lower frequen-  
 597 cies, when sonicating with plane waves, antibubbles may perform better than SonoVue™.  
 598 Moreover, if made smaller for a clinical application, the antibubble resonance frequency is  
 599 expected to increase, leading to even greater higher harmonic generation at 3.5 MHz. Figure  
 600 9 also illustrates that in cases when small quantities of contrast agent are distributed in  
 601 a vascular network, in contrast to the scatter measurement, antibubble attenuation of 4.4  
 602 dB/cm does not degrade the images in a perceivable manner.

603 In comparison to commercial UCAs, the studied endoskeleton antibubbles are larger<sup>1,35</sup>.  
 604 A size below 7  $\mu\text{m}$  in diameter is recommended for UCA bubbles<sup>35</sup>, about half the size of the  
 605 largest endoskeleton antibubbles in the studied suspensions (Fig. 2). The shell thickness of  
 606 commercial UCAs ranges from 2 to 200 nm<sup>1,16,25,68</sup>, with SonoVue™ having a particularly  
 607 thin and compliant shell of about 4 nm<sup>25</sup>. The silica shell of antibubbles is stiff and about 1  
 608  $\mu\text{m}$  thick, based on brightfield microscopy images of antibubbles with the same shell<sup>7</sup>. **The**  
 609 **shell properties greatly contribute to UCA attenuation<sup>11,43</sup>, suggesting a study of alternative**  
 610 **compliant materials for the antibubble shell that would reduce shadowing effects associated**  
 611 **with high antibubble attenuation.** Current generation contrast agents such as SonoVue™

612 and Definity<sup>TM</sup> typically contain low solubility gas, providing a longer bubble lifetime. The  
613 studied endoskeleton bubbles contain highly soluble air. No endoskelton or core structures  
614 are present in any of the currently approved contrast agents.

## 615 V. Conclusions

616 Based on previous work, antibubbles, i.e., encapsulated gas bubbles with incompressible  
617 cores, are expected to demonstrate augmented nonlinear behavior compared to encapsulated  
618 gas bubbles. This opens the door to improving CE-US image quality and to a traceable ther-  
619 apeutic agent with large ammounts of therapeutic compounds in the core. This work aimed  
620 at characterizing the nonlinear behavior of endoskeletal antibubbles, an antibubble UCA  
621 prototype, and comparing it to reference bubbles and a commercially available and clinically  
622 approved UCA, SonoVue<sup>TM</sup>, in the range of diagnostic frequencies from 1 to 3.5 MHz and  
623 pressures comparable to those employed clinically at  $MI = 0.2$  and  $MI = 0.3$ .

624 We demonstrated that the studied dispersions of endoskeletal antibubbles generate com-  
625 parable or greater higher harmonic content than those composed of reference bubbles with an  
626 equivalent median diameter and smaller SonoVue<sup>TM</sup> bubbles. Higher harmonics comparable  
627 to that of SonoVue<sup>TM</sup> at a high concentration may be attributed to a larger antibubble size,  
628 a different shell and gas. Figure 7 mitigates the influence of bubble concentration and bubble  
629 size on the scattered spectra. However, the signals scattered by the UCAs in the focal spot  
630 may have been attenuated by the surrounding UCA. Therefore, the advantage of antibubbles  
631 over other contrast agents may have been masked in Fig. 7 by their higher attenuation. The  
632 plane-wave DCE-US measurement, simulating clinical imaging at 3.5 MHz, demonstrated  
633 that antibubbles have comparable performance to SonoVue<sup>TM</sup> at a high concentration at  
634 a frequency close to its resonance frequency, and superior performance, compared to the  
635 reference bubbles.

636 Based on this work, it is difficult to draw the solid conclusion that the incompressible  
637 core leads to greater higher harmonic generation, due to the differences in the size distri-  
638 butions (Fig. 2) and inner bubble content of the studied antibubbles and reference bubbles  
639 (Fig. 1). The stronger higher harmonics of antibubbles, compared to reference bubbles  
640 may also be attributed to the lower resonance frequency of the reference bubble dispersion.

641 To present proof that antibubbles have an advantage over bubble-based contrast agents for  
642 imaging purposes, other reference bubbles are required, identical to antibubbles in all as-  
643 pects, except for the core. Such an agent is currently not available. Nevertheless, we present  
644 evidence that endoskeletal antibubbles demonstrate strong nonlinear behavior at frequencies  
645 from 1 to 3.5 MHz. These results are encouraging and suggest that antibubbles hold high  
646 potential to serve as traceable therapeutic agents. For this purpose, the solid core would  
647 have to be replaced by a liquid inclusion with medication.

## 648 VI. Acknowledgements

649 This work was supported by eMTIC collaboration and partly by the National Research  
650 Foundation of South Africa, Grant Number 127102. We thank Anton Nikolaev for the  
651 design of the molds utilized for the cuvette preparation.

652

653 <sup>1</sup> A. Novell, J. M. Escoffre, and A. Bouakaz, Ultrasound contrast imaging in cancer-  
654 technical aspects and prospects, *Curr. Mol. Imaging* **2**, 77–88 (2013).

655 <sup>2</sup> R. J. G. van Sloun, L. Demi, A. W. Postema, J. J. de la Rosette, H. Wijkstra, and  
656 M. Mischi, Ultrasound-contrast-agent dispersion and velocity imaging for prostate cancer  
657 localization, *Med. Image Anal.* **35**, 610–619 (2017).

658 <sup>3</sup> M. P. J. Kuenen, M. Mischi, and H. Wijkstra, Contrast-ultrasound diffusion imaging  
659 for localization of prostate cancer, *IEEE Trans. Med. Imag.* **30**, 1493–1502 (2011).

660 <sup>4</sup> S. Turco, H. Wijkstra, and M. Mischi, Mathematical models of contrast transport  
661 kinetics for cancer diagnostic imaging: a review, *IEEE Rev. Biomed. Eng.* **9**, 121–147  
662 (2017).

663 <sup>5</sup> D. T. Fetzer, V. Rafailidis, C. Peterson, E. G. Grant, P. Sidhu, and R. G. Barr, Artifacts  
664 in contrast-enhanced ultrasound: a pictorial essay, *Abdom. Radiol.* **43**, 977–997 (2018).

665 <sup>6</sup> A. T. Poortinga, Micron-sized antibubbles with tunable stability, *Colloids Surf. A* **419**,  
666 15–20 (2013).

667 <sup>7</sup> N. Kudo, R. Uzbekov, R. Matsumoto, R. Shimizu, C. S. Carlson, N. Anderton, A. Der-  
668 ouchaix, C. Penny, A. T. Poortinga, D. M. Rubin, A. Bouakaz, and M. Postema, Asym-  
669 metric oscillations of endoskeletal antibubbles, *Jpn. J. Appl. Phys.* **59**, SKKE02 (2020).

670 <sup>8</sup> C. A. Sennoga, E. Kanbar, L. Auboire, P. A. Dujardin, D. Fouan, J. M. Escoffre, and  
671 A. Bouakaz, Microbubble-mediated ultrasound drug-delivery and therapeutic monitor-  
672 ing, *Expert Opin. Drug Deliv.* **14**, 1031–1043 (2017).

673 <sup>9</sup> E. P. Stride and C. C. Coussios, Cavitation and contrast: the use of bubbles in ultrasound  
674 imaging and therapy, *Proc. Inst. Mech. Eng. H* **224**, 171–191 (2009).

675 <sup>10</sup> O. F. Kaneko and J. K. Willmann, Ultrasound for molecular imaging and therapy in  
676 cancer, *Quant. Imaging Med. Surg.* **2**, 87–97 (2012).

677 <sup>11</sup> C. C. Church, The effects of an elastic solid surface layer on the radial pulsations of gas  
678 bubbles, *J. Acoust. Soc. Am.* **97**, 1510–1521 (2009).

- 679 <sup>12</sup> N. de Jong, R. Cornet, and C. T. Lancée, Higher harmonics of vibrating gas-filled  
680 microspheres. Part two: measurements, *Ultrasonics* **32**, 455–459 (1994).
- 681 <sup>13</sup> C. F. Dietrich et al., How to perform contrast-enhanced ultrasound (CEUS), *Ultrasound*  
682 *Int. Open* **4**, E2 (2018).
- 683 <sup>14</sup> R. C. Gessner, C. B. Frederick, F. S. Foster, and P. A. Dayton, Acoustic angiography:  
684 a new imaging modality for assessing microvasculature architecture, *Int. J. Biomed.*  
685 *Imaging* **2013**, 1–9 (2013).
- 686 <sup>15</sup> T. Lorentzen, C. Nolsøe, C. Ewertsen, M. Nielsen, E. Leen, R. Havre, N. Gritzmann,  
687 B. Brkljacic, D. Nürnberg, A. Kabaalioglu, D. Strobel, C. Jessen, F. Piscaglia, O. H.  
688 Gilja, P. S. Sidhu, and C. F. Dietrich, EFSUMB guidelines on interventional ultrasound  
689 (INVUS), part I–general aspects (long version), *Ultraschall Med.* **36**, E1–E14 (2015).
- 690 <sup>16</sup> J.-M. Correas, L. Bridal, A. Lesavre, A. Méjean, M. Claudon, and O. Hélénon, Ultra-  
691 sound contrast agents: properties, principles of action, tolerance, and artifacts, *Eur.*  
692 *Radiol.* **11**, 1316–1328 (2001).
- 693 <sup>17</sup> F. Forsberg, W. T. Shi, and B. Goldberg, Subharmonic imaging of contrast agents,  
694 *Ultrasonics* **38**, 93–98 (2000).
- 695 <sup>18</sup> A. Novell, J.-M. Escoffre, and A. Bouakaz, Second harmonic and subharmonic for non-  
696 linear wideband contrast imaging using a capacitive micromachined ultrasonic transducer  
697 array, *Ultrasound Med. Biol.* **39**, 1500–1512 (2013).
- 698 <sup>19</sup> S. Dorbolo, H. Caps, and N. Vandewalle, Fluid instabilities in the birth and death of  
699 antibubbles, *New J. Phys.* **5**, 74–77 (2003).
- 700 <sup>20</sup> M. Postema, F. J. ten Cate, G. Schmitz, N. de Jong, and A. van Wamel, Generation of  
701 a droplet inside a microbubble with the aid of an ultrasound contrast agent: first result,  
702 *Lett. Drug. Des. Discov.* **4**, 74–77 (2007).
- 703 <sup>21</sup> S. Kotopoulis, K. Johansen, O. H. Gilja, A. T. Poortinga, and M. Postema, Acoustically  
704 active antibubbles, *Acta Phys. Pol. A* **127**, 99–102 (2015).
- 705 <sup>22</sup> M. Postema and O. H. Gilja, Ultrasound-directed drug delivery, *Curr. Pharm. Biotech-*  
706 *nol.* **8**, 355–361 (2007).
-



- 707 <sup>23</sup> M. Postema, A. Novell, C. Sennoga, A. T. Poortinga, and A. Bouakaz, Harmonic  
708 response from microscopic antibubbles, *Appl. Acoust.* **137**, 148–150 (2018).
- 709 <sup>24</sup> N. Anderton, Acoustic properties of antibubbles, Dissertation, University of the Wit-  
710 watersrand, Johannesburg, 2020.
- 711 <sup>25</sup> J. Tu, J. Guan, Y. Qiu, and T. J. Matula, Estimating the shell parameters of SonoVue®  
712 microbubbles using light scattering, *J. Acoust. Soc. Am.* **126**, 2954–2962 (2009).
- 713 <sup>26</sup> L. Hoff, Acoustic characterization of contrast agents for medical ultrasound imaging,  
714 Springer, Heidelberg, 2001.
- 715 <sup>27</sup> M. Schneider, Characteristics of SonoVue™, *Echocardiography* **16**, 743–746 (1999).
- 716 <sup>28</sup> A. Boukaz, N. de Jong, and C. Cachard, Standard properties of ultrasound contrast  
717 agents, *Ultrasound Med. Biol.* **24**, 469–472 (1998).
- 718 <sup>29</sup> J. M. Gorce, M. Arditì, and M. Schneider, Influence of bubble size distribution on the  
719 echogenicity of ultrasound contrast agents, *Invest. Radiol.* **35**, 661–671 (2000).
- 720 <sup>30</sup> N. de Jong, M. Emmer, A. van Wamel, and M. Versluis, Ultrasonic characterization of  
721 ultrasound contrast agents, *Med. Biol. Eng. Comput.* **47**, 861–873 (2009).
- 722 <sup>31</sup> T. K. Kim, H. J. Jang, P. N. Burns, J. Murphy-Lavallee, and S. R. Wilson, Focal  
723 nodular hyperplasia and hepatic adenoma: differentiation with low mechanical-index  
724 contrast-enhanced sonography, *Am. J. Roentgenol.* **190**, 58–66 (2008).
- 725 <sup>32</sup> C. F. Dietrich, J. C. Mertens, B. Braden, G. Schuessler, M. Ott, and A. Ignee, Contrast-  
726 enhanced ultrasound of histologically proven liver hemangiomas, *Hepatology* **45**, 1139–  
727 1145 (2007).
- 728 <sup>33</sup> H. Maruyama, M. Takashi, H. Ishibashi, H. Okugawa, S. Okabe, M. Yoshikawa, and  
729 O. Yokosuka, Ultrasound-guided treatments under low acoustic power contrast harmonic  
730 imaging for hepatocellular carcinomas undetected by B-mode ultrasonography, *Liver Int.*  
731 **29**, 708–714 (2008).
- 732 <sup>34</sup> M. Postema and O. H. Gilja, Contrast-enhanced and targeted ultrasound, *World J.*  
733 *Gastroenterol.* **17**, 28–41 (2005).

- 734 <sup>35</sup> D. Cosgrove, Ultrasound contrast agents: an overview, *Eur. J. Radiol.* , 324 – 330  
735 (2006).
- 736 <sup>36</sup> B. Zeqiri, Errors in attenuation measurements due to nonlinear propagation effects, *J.*  
737 *Acoust. Soc. Am.* **91**, 2585–2593 (1992).
- 738 <sup>37</sup> P. J. A. Frinking, A. Bouakaz, J. Kirkhorn, F. J. ten Cate, and N. de Jong, Ultrasound  
739 contrast imaging: current and new potential methods, *Ultrasound Med. Biol.* **26**, 965–  
740 975 (2000).
- 741 <sup>38</sup> T. Segers, N. de Jong, and M. Versluis, Uniform scattering and attenuation of acousti-  
742 cally sorted ultrasound contrast agents: modeling and experiments, *J. Acoust. Soc. Am.*  
743 **140**, 2506–2517 (2016).
- 744 <sup>39</sup> M. Lampaskis and M. Averkiou, Investigation of the relationship of nonlinear backscat-  
745 tered ultrasound intensity with microbubble concentration at low MI, *Ultrasound Med.*  
746 *Biol.* **36**, 306–312 (2010).
- 747 <sup>40</sup> P. Chen, S. Turco, R. J. G. van Sloun, A. Pollet, J. den Toonder, H. Wijkstra, and  
748 M. Mischi, In-vitro investigation of the relationship between microvascular structure  
749 and ultrasound contrast agent dynamics, *Proc. 2019 IEEE Int. Ultrason. Symp.* , 403–  
750 406 (2019).
- 751 <sup>41</sup> H. J. Bleeker, K. K. Shung, and J. L. Barnhart, Ultrasonic characterization of Albunex,  
752 a new contrast agent, *J. Acoust. Soc. Am.* **87**, 1792–1797 (1990).
- 753 <sup>42</sup> P. J. A. Frinking and N. de Jong, Acoustic modeling of shell-encapsulated gas bubbles,  
754 *Ultrasound Med. Biol.* **24**, 523–533 (1998).
- 755 <sup>43</sup> N. de Jong, L. Hoff, T. Skotland, and N. Bom, Absorption and scatter of encapsulated  
756 gas filled microspheres: theoretical considerations and some measurements, *Ultrasonics*  
757 **30**, 95–103 (1992).
- 758 <sup>44</sup> M. Emmer, H. J. Vos, D. E. Goertz, A. van Wamel, M. Verluis, and N. de Jong, Pressure-  
759 dependent attenuation and scattering of phospholipid-coated microbubbles at low acous-  
760 tic pressures, *Ultrasound Med. Biol.* **35**, 102–111 (2009).
-

- 761 <sup>45</sup> T. Grandke, Interpolation algorithms for discrete fourier transforms of weighted signals,  
762 IEEE Trans. Instrum. Meas. **32**, 350–355 (1983).
- 763 <sup>46</sup> H. X. Xu, M. D. Lu, G. J. Liu, X. Y. Xie, Z. F. Xu, Y. L. Zheng, and J. Y. Liang,  
764 Imaging of peripheral cholangiocarcinoma with low-mechanical index contrast-enhanced  
765 sonography and Sonovue, J. Ultrasound Med. , 23–33 (2006).
- 766 <sup>47</sup> P. Ricci, A. Laghi, V. Cantisani, P. Paolantonio, S. Pacella, E. Pagliara, F. Arduini,  
767 V. Pasqualini, F. Trippa, M. Filpo, and R. Passariello, Contrast-enhanced sonography  
768 with SonoVue: enhancement patterns of benign focal liver lesions and correlation with  
769 dynamic gadobenate dimeglumine-enhanced MRI, Am. J. Roentgenol. , 821–827 (2005).
- 770 <sup>48</sup> M. X. Tang, R. J. Eckersley, and J. A. Noble, Pressure-dependent attenuation with  
771 microbubbles at low mechanical index, Ultrasound Med. Biol. **31**, 377–384 (2005).
- 772 <sup>49</sup> U. Techavipoo, T. Varghese, Q. Chen, T. A. Stiles, J. A. Zagzebski, and G. R. Frank,  
773 Temperature dependence of ultrasonic propagation speed and attenuation in excised  
774 canine liver tissue measured using transmitted and reflected pulses, J. Acoust. Soc. Am.  
775 **115**, 2859–2865 (2004).
- 776 <sup>50</sup> T. Faez, D. Goertz, and N. de Jong, Characterization of Definity™ ultrasound contrast  
777 agent at frequency range of 5–15 MHz, Ultrasound Med. Biol. **37**, 338–342 (2011).
- 778 <sup>51</sup> T. Segers, P. Kruizinga, M. P. Kok, G. Lajoinie, N. de Jong, and M. Versluis, Monodis-  
779 perse versus polydisperse ultrasound contrast agents: non-linear response, sensitivity,  
780 and deep tissue imaging potential, Ultrasound Med. Biol. **44**, 1482–1492 (2018).
- 781 <sup>52</sup> R. Chanamai and D. J. McClements, Ultrasonic attenuation of edible oils, J. Am. Oil  
782 Chem. Soc. **75**, 1447–1448 (1998).
- 783 <sup>53</sup> J. A. Kopechek, K. J. Haworth, J. L. Raymond, T. D. Mast, S. R. Perrin, M. E.  
784 Klegerman, S. Huang, T. M. Porter, D. D. McPherson, and C. K. Holland, Acoustic  
785 characterization of echogenic liposomes: frequency-dependent attenuation and backscat-  
786 ter, J. Acoust. Soc. Am. **130**, 3472–3481 (2011).
- 787 <sup>54</sup> J. C. V. Schwarz, M. G. J. T. B. van Lier, J. P. H. M. van den Wijngaard, M. Siebes,  
788 and E. van Bavel, Topologic and Hemodynamic Characteristics of the Human Coronary  
789 Arterial Circulation, Front. Physiol. **10**, 1611 (2020).

- 790 <sup>55</sup> M. I. Qamar, A. E. Read, R. Skidmore, J. M. Evans, and P. N. Wells, Transcutaneous  
791 Doppler ultrasound measurement of superior mesenteric artery blood flow in man, *Gut*  
792 **27**, 100–105 (1986).
- 793 <sup>56</sup> J. H. Lee, H. Cheong, S. S. Lee, C. K. Lee, Y. S. Sung, J.-W.Huh, J.-A. Song, and  
794 H. Choe, Perfusion assessment using intravoxel incoherent motion-based analysis of  
795 diffusion-weighted magnetic resonance imaging: validation through phantom experi-  
796 ments, *Invest. Radiol.* **51**, 520–528 (2016).
- 797 <sup>57</sup> M. E. Kamphuis, M. J. W. Greuter, R. H. J. A. Slart, and C. H. Slump, Quantitative  
798 imaging: systematic review of perfusion/flow phantoms, *Eur. Radiol. Exp.* **4**, 1–13  
799 (2020).
- 800 <sup>58</sup> R. J. Eckersley, C. T. Chin, and P. N. Burns, Optimising phase and amplitude modula-  
801 tion schemes for imaging microbubble contrast agents at low acoustic power, *Ultrasound*  
802 *Med. Biol.* **31**, 213–219 (2005).
- 803 <sup>59</sup> R. K. Millard, Indicator-dilution dispersion models and cardiac output computing meth-  
804 ods, *Am. Physiol. Soc.* **272**, H2004–H2012 (1997).
- 805 <sup>60</sup> A. Lopatzidis and R. K. Millard, Empirical estimators of gamma fits to tracer dilution  
806 curves and their technical basis and practical scope, *Phys. Meas.* **22**, N1–N5 (2001).
- 807 <sup>61</sup> M. Postema and G. Schmitz, Bubble dynamics involved in ultrasonic imaging, *Expert*  
808 *Rev. Mol. Diagn.* **6**, 493–502 (2006).
- 809 <sup>62</sup> W.-S. Chen, T. J. Matula, A. A. Brayman, and L. A. Crum, A comparison of the  
810 fragmentation thresholds and inertial cavitation doses of different ultrasound contrast  
811 agents, *J. Acoust. Soc. Am.* **113**, 643–651 (2003).
- 812 <sup>63</sup> D. E. Goertz, N. de Jong, and A. F. van der Steen, Attenuation and size distribution  
813 measurements of Definity™ and manipulated Definity™ populations, *Ultrasound Med.*  
814 *Biol.* **33**, 1376–1388 (2007).
- 815 <sup>64</sup> M. X. Tang and R. J. Eckersley, Frequency and pressure dependent attenuation and  
816 scattering by microbubbles, *Ultrasound Med. Biol.* **33**, 164–168 (2007).
-

- 817 <sup>65</sup> X. Gong, D. Zhang, J. Liu, H. Wang, Y. Yan, and X. Xu, Study of acoustic nonlinearity  
818 parameter imaging methods in reflection mode for biological tissues, *J. Acoust. Soc.*  
819 *Am.* **116**, 1819–1825 (2004).
- 820 <sup>66</sup> G. ter Haar, Ultrasonic imaging: safety considerations, *Interface Focus* **1**, 686–697  
821 (2011).
- 822 <sup>67</sup> M. Postema, R. Matsumoto, R. Shimizu, A. T. Poortinga, and N. Kudo, High-speed  
823 footage shows transient nucleation of different hydrophobic particles in suspension, *Jpn.*  
824 *J. Appl. Phys.* **59**, SKKD07 (2020).
- 825 <sup>68</sup> P. Frinking, T. Segers, Y. Luan, and F. Tranquart, Three decades of ultrasound contrast  
826 agents: a review of the past, present and future improvements, *Ultrasound Med. Biol.*  
827 **46**, 892–908 (2020).